

Bayesian inference on the order of stationary vector autoregressions

Rachel L. Binks¹, Sarah E. Heaps^{*2}, Mariella Panagiotopoulou³, Yujiang Wang³,
and Darren J. Wilkinson²

¹School of Mathematics, Statistics and Physics, Newcastle University

²Department of Mathematical Sciences, Durham University

³School of Computing, Newcastle University

Abstract

All vector autoregressive models have an associated order p ; conditional on observations at the preceding p time points, the variable at time t is conditionally independent of all the earlier history of the process. Learning the order of the model is therefore vital for its characterisation and subsequent use in forecasting. It is common to assume that a vector autoregression is stationary. This prevents the predictive variance of the process from increasing without bound as the forecast horizon increases and facilitates various interpretations of the relationships between variables. A vector autoregression is stable if and only if the roots of its characteristic equation lie outside the unit circle, which constrains the autoregressive coefficient matrices to lie in the stationary region. Unfortunately, the geometry of the stationary region can be very complicated, and specification of a prior distribution over this region is therefore difficult. In this work, the autoregressive coefficients are mapped to a set of transformed partial autocorrelation matrices which are unconstrained, allowing for straightforward prior specification, routine computational inference, and meaningful interpretation of the magnitude of the elements in the matrix. The multiplicative gamma process is used to build a prior distribution for the unconstrained matrices, which encourages increasing shrinkage of the partial autocorrelation parameters as the lag increases. Identifying the lag beyond which the partial autocorrelations become equal to zero then determines the order of the process. Posterior inference is performed using Hamiltonian Monte Carlo via the probabilistic programming language Stan. A truncation criterion is used to determine whether a partial autocorrelation matrix has been effectively shrunk to zero. The value of the truncation threshold is motivated by classical theory on the sampling distribution of the partial autocorrelation function. The work is applied in a simulation study to investigate the agreement between the posterior distribution for the order of the process and its known value, with promising results. The model and inferential procedures are then applied to neural activity data in order to investigate ultradian rhythms in the brain.

1 Introduction

Vector autoregressive (VAR) processes are widely used to model multivariate time-series data in a variety of fields including neuroscience (Chiang et al., 2016), bioinformatics (Jiang et al., 2013; Hannaford et al., 2023), macroeconomics (Koop and Korobilis, 2010),

*Corresponding author: sarah.e.heaps@durham.ac.uk

and energy economics (Heaps et al., 2020). In an autoregression of order p , the random variable at time t is conditionally independent of its values at lags $p + 1, p + 2, \dots$ given observations at the preceding p time points. Indeed the random variable at time t can be expressed as a noisy linear combination of these p values. The order of the autoregression is therefore intrinsic to the characterisation of the joint model for the process. However, its value is typically not known *a priori*.

A common assumption when working with Gaussian time-series data is that of stationarity, which posits that the means, variances and covariances of the process do not change over time. Since the overall level of many time-series exhibits periodic or systematic variation due to seasonality or time-trends, stationarity is often implausible as an assumption when modelling the raw data. However, stationary vector autoregressions frequently form the core building block of more sophisticated models, for example for differenced data in integrated models, for innovations from a time-varying mean in a time-series regression model or simply as components in state space models which are thought to be mean-reverting. Stationarity can be enforced in vector autoregressions by restricting the autoregressive coefficient matrices to lie within a subset of the parameter space called the stationary region. From a practical perspective, this prevents the predictive variance of the process from growing without bound into the future. This is often keenly motivated, for instance in applications where the goal is long-term forecasting or when modelling the dynamics of a linear system which is assumed to be in its equilibrium distribution. Moreover, stationarity admits various interpretations of the relationships between variables through the infinite-order moving average representation of the process, for example through Granger causality networks or impulse response analysis.

In the context of univariate stationary autoregressions, Bayesian inference on the order of the process has been widely studied. Reparameterising the model in terms of its partial autocorrelations, Barnett et al. (1996) enforce stationarity by restricting the support of each partial autocorrelation parameter to the interval $(-1, 1)$. A univariate stationary autoregression of order p has a non-zero partial autocorrelation at lag p and then zero partial autocorrelations at all higher lags. Therefore, by choosing a large (maximum) value for p and assigning each partial autocorrelation a spike-and-slab prior with a continuous distribution over $(-1, 1)$ and an atom of probability at zero, the authors allow inference on the order of the process. Vermaak et al. (2004) use the same reparameterisation of the model to enforce stationarity but frame the problem of order determination as a model selection problem and use reversible jump Markov chain Monte Carlo to learn the order of the process. In Huerta and West (1999), stationarity is enforced through a different reparameterisation of the autoregression in terms of the reciprocal roots of its characteristic equation. Under this parameterisation, the process is stationary if and only if the reciprocal roots have moduli less than 1 and the order of the process is determined by the number of reciprocal roots with non-zero modulus. Priors are assigned to the real and complex reciprocal roots with atoms of probability at moduli 0 in each case, thereby allowing inference on the model order.

Due to the geometric complexities of the stationary region in the multivariate case, extensions of these ideas to learning the order of stationary *vector* autoregressions are rare. Indeed, efforts to enforce stationarity in Bayesian analyses of vector autoregressions have, until recently, been thwarted by the geometry of the stationary region; see Roy et al. (2019) and Heaps (2023) for the state-of-the-art. An exception is the work of Huerta and Prado (2006) who extend Huerta and West (1999) by considering a multivariate generalisation of the characteristic equation. However, because this is only available when the autoregressive matrices are diagonal, their work is limited to the class of diagonal

vector autoregressive processes. Other recent work which addresses the problem of order determination in vector autoregressions includes Zhang et al. (2021) and Fan et al. (2022) in which the autoregressive coefficient matrices are structured into a three-way tensor to facilitate structural dimension reduction. A low rank tensor decomposition is then applied, in which one margin determines the order of the model, with shrinkage process priors used to encourage parsimony. Clearly, however, these tensor models are not fully flexible if dimension reduction is imposed, being limited to subsets of the class of all vector autoregressions. Moreover, stationarity is not enforced.

In earlier work, Heaps (2023) established a methodology for enforcing stationarity through the prior in vector autoregressions based on an unconstrained reparameterisation of the stationary model. This is constructed by mapping the original model parameters to a set of partial autocorrelation matrices and then applying a second transformation which simply scales the singular values of each of these partial autocorrelation matrices from $[0, 1)$ to the positive real line. The transformed partial autocorrelation matrices are interpretable and allow specification of a prior which is invariant with respect to the order of the components in the observation vector. Markov chain Monte Carlo (MCMC) methods for computational inference need only operate over a Euclidean space, making implementation routine, for example using Hamiltonian Monte Carlo through probabilistic programming software like Stan. However, a clear limitation with this approach is that inference is conditional on a specified value for the model order, with no account for the associated uncertainty. In this work, we provide an extension to the prior and associated procedures for computational inference which allows the order to be another unknown quantity in the model.

A Bayesian approach to quantifying uncertainty on the dimension of nested models is to fit an overparameterised model with purposefully more components than are required. By using a shrinkage prior, components that are shrunk enough to be deemed negligible in the likelihood can then be discarded. Consequently, inference on both the continuous model parameters and the model dimension are available from a single within-model MCMC sampler, without recourse to transdimensional MCMC; see, for instance, Rousseau and Mengersen (2011) and Bhattacharya and Dunson (2011) in the context of mixture and factor models, respectively. Borrowing ideas from this literature, we construct a prior which increasingly shrinks the transformed partial autocorrelation matrices at higher lags towards zero and allows assessment of the lag beyond which the partial autocorrelations become essentially equal to zero. This determines the order of the process. The interpretability of the reparameterised model allows classical theory on the sampling distribution of the partial autocorrelation function to inform specification of the shrinkage prior and subsequent decision-making. To the best of our knowledge, this is the first work in the literature to address the problem of order determination from a Bayesian perspective in the general class of stationary vector autoregressions. We provide code for implementation of computational inference via Stan thereby facilitating use by a variety of practitioners across the spectrum of fields which rely on vector autoregressions for modelling and forecasting applications.

The remainder of the paper is structured as follows. In Section 2 we discuss a reparameterisation of stationary vector autoregressive models in terms of a set of interpretable, unconstrained parameters. In Section 3 we discuss the prior distribution assigned to the unknowns in our reparameterised model. Section 4 considers posterior inference and the use of a truncation criterion to determine model order. In Section 5 we apply our model and inferential procedures in a set of simulation experiments before considering an application to neural activity data in Section 6. Finally Section 7 provides some concluding

remarks.

2 Stationary vector autoregressions

2.1 Vector autoregressions

Without loss of generality, suppose that the m -variate process $\{\mathbf{y}_t\}$ can be modelled as a zero-mean vector autoregression of order p , denoted $\text{VAR}_m(p)$,

$$\mathbf{y}_t = \phi_1 \mathbf{y}_{t-1} + \dots + \phi_p \mathbf{y}_{t-p} + \boldsymbol{\epsilon}_t, \quad (1)$$

where the errors $\boldsymbol{\epsilon}_t$ form a sequence of uncorrelated, zero-mean multivariate normal random vectors, $\boldsymbol{\epsilon}_t \sim N_m(\mathbf{0}, \Sigma)$. The continuous model parameters therefore comprise the autoregressive coefficient matrices $\phi_i \in M_{m \times m}(\mathbb{R})$, $i = 1, \dots, p$, which are denoted collectively as $\Phi \in M_{m \times m}(\mathbb{R})^p$, and the error variance matrix $\Sigma \in \mathcal{S}_m^+$, where $M_{m \times n}(V)$ and \mathcal{S}_m^+ denote the space of $m \times n$ matrices with entries in V and the space of $m \times m$ symmetric, positive definite matrices, respectively. Defining B as the backshift operator, such that $B^k \mathbf{y}_t = \mathbf{y}_{t-k}$, it is common to express (1) as

$$\boldsymbol{\epsilon}_t = (I_m - \phi_1 B - \dots - \phi_p B^p) \mathbf{y}_t = \phi(B) \mathbf{y}_t,$$

in which I_m is the $m \times m$ identity matrix and $\phi(u) = (I_m - \phi_1 u - \dots - \phi_p u^p)$, $u \in \mathbb{C}$, is referred to as the characteristic polynomial. A vector autoregression is stable if and only if all the roots of $\det\{\phi(u)\} = 0$ lie outside the unit circle. Since all stable processes are stationary, and unstable stationary processes are not generally of interest, this is often referred to as the stationarity condition for Φ and the subset of $M_{m \times m}(\mathbb{R})^p$ over which the condition is satisfied is referred to as the stationary region, denoted $\mathcal{C}_{p,m}$.

2.2 Reparameterisation over the stationary region

The geometry of the stationary region $\mathcal{C}_{p,m}$ becomes increasingly complex as either p or m increase. With no standard distributions over $\mathcal{C}_{p,m}$, this complicates the process of specifying a prior that conveys meaningful information, for example, concerning the relative sizes of the autocorrelations at different lags. Moreover, it is difficult to design an efficient MCMC sampler which targets a distribution with support constrained to $\mathcal{C}_{p,m}$. In recent work, Heaps (2023) proposes a solution which addresses both issues, reparameterising the model over the stationary region in terms of a set of interpretable, unconstrained parameters. The reparameterisation involves two bijective mappings. First, the original model parameters $(\Sigma, \Phi) \in \mathcal{S}_m^+ \times \mathcal{C}_{p,m}$ are mapped to a new parameter set $\{\Sigma, (P_1, \dots, P_p)\} \in \mathcal{S}_m^+ \times \mathcal{V}^p$ in which \mathcal{V} denotes the subset of matrices in $M_{m \times m}(\mathbb{R})$ whose singular values are less than one. The matrix P_{s+1} is referred to as the $(s+1)$ -th partial autocorrelation matrix. It is defined as the conditional cross-covariance matrix between \mathbf{y}_{t+1} and \mathbf{y}_{t-s} given $\mathbf{y}_t, \dots, \mathbf{y}_{t-s+1}$ which has been standardised through

$$P_{s+1} = \Sigma_s^{-1/2} \text{Cov}(\mathbf{y}_{t+1}, \mathbf{y}_{t-s} | \mathbf{y}_t, \dots, \mathbf{y}_{t-s+1}) \Sigma_s^{*-1/2},$$

$s = 0, \dots, p-1$, in which Σ_s and Σ_s^* are the conditional variances

$$\Sigma_s = \text{Var}(\mathbf{y}_{t+1} | \mathbf{y}_t, \dots, \mathbf{y}_{t-s+1}) \quad \text{and} \quad \Sigma_s^* = \text{Var}(\mathbf{y}_{t-s} | \mathbf{y}_{t-s+1}, \dots, \mathbf{y}_t)$$

and $\Sigma^{1/2}$ denotes the symmetric matrix-square root. Full details of the mapping and its inverse, which proceed by recursion, are described in Heaps (2023).

A second transformation then maps each partial autocorrelation matrix $P \in \mathcal{V}$ to an unconstrained square matrix $A \in M_{m \times m}(\mathbb{R})$ through

$$A = (I_m - PP^T)^{-1/2}P.$$

Denoting the singular value decomposition of P by $P = U\text{diag}(r_1, \dots, r_m)V^T$ in which the singular values satisfy $1 > r_1 \geq r_2 \geq \dots \geq r_m \geq 0$, the corresponding factorisation of A is given by $A = U\text{diag}(\tilde{r}_1, \dots, \tilde{r}_m)V^T$ where $\tilde{r}_i = r_i/(1 - r_i^2)^{1/2} \geq 0$, $i = 1, \dots, m$. Therefore the second transformation can be regarded as an orientation-preserving mapping which simply scales the singular values of P from $[0, 1)$ to the positive real line.

3 Prior distribution

3.1 Shrinkage prior for transformed partial autocorrelations

The relationship between the singular value decompositions of P and A , described in the previous section, has two important implications. First, the spectral norms of P and A , $r_1 = \|P\|_2$ and $\tilde{r}_1 = \|A\|_2$, are clearly related through the monotonic mapping: $\tilde{r}_1 = r_1/(1 - r_1^2)^{1/2}$. The relative sizes of the unconstrained parameters A_s across lags $s = 1, \dots, p$ therefore relate directly to the relative sizes of the partial autocorrelation matrices P_s across lags. Second, $P = o_m$ if and only if $A = o_m$ in which o_m denotes the $m \times m$ matrix of zeros. It follows from the definition of the partial autocorrelation matrices that for $k < p$, $P_k \neq o_m$ and $P_{k+s} = o_m$ for $s = 1, \dots, p - k$ if and only if $\phi_k \neq o_m$ and $\phi_{k+s} = o_m$ for $s = 1, \dots, p - k$. The order of a VAR $_m(p)$ process is therefore $k < p$ if and only if $A_k \neq o_m$ and $A_{k+s} = o_m$ for $s = 1, \dots, p - k$. Under the unconstrained parameterisation, it follows that the model of order $k < p$ is nested within the model of order $k + 1$. As discussed in Section 1, we can therefore borrow ideas from the literature on overfitted models by adopting a shrinkage prior for $A_1, \dots, A_{p_{\max}}$ with a large value for p_{\max} . This allows learning about the lag beyond which the A_s can be taken as zero matrices, thereby informing inference on the order p of the process. It can therefore be regarded as an extension of the prior in the univariate case that uses spike-and-slab distributions for the partial autocorrelation parameters (Barnett et al., 1996). Moreover, we can convey the very reasonable idea that the partial autocorrelations at higher lags are likely to be smaller than those at lower lags by choosing a shrinkage prior for the A_s , $s = 1, \dots, p_{\max}$, whose degree of shrinkage increases with the lag s .

A popular increasing shrinkage prior is the multiplicative gamma process (MGP) (Bhattacharya and Dunson, 2011) originally developed as a structured sequence of global-local shrinkage priors for the loadings matrix in infinite factor models. Denoting the (i, j) th element in A_s by $a_{s,ij}$ we adopt a prior of this form by choosing

$$a_{s,ij} | \lambda_{s,ij}, \tau_s \sim N(0, \lambda_{s,ij}^{-1} \tau_s^{-1}),$$

independently for $i, j = 1, \dots, m$, $s = 1, \dots, p_{\max}$, where the local precision parameters at lag s are assigned the prior

$$\lambda_{s,ij} \sim \text{Gam}(a/2, a/2),$$

independently for $i, j = 1, \dots, m$, $s = 1, \dots, p_{\max}$, and the global precision parameter at lag s is constructed as

$$\tau_s = \prod_{k=1}^s \delta_k, \quad \delta_1 \sim \text{Gam}(a_1, 1), \quad \delta_k \sim \text{Gam}(a_2, 1), \quad k \geq 2$$

in which the δ_k are independent. The global precisions τ_s are therefore a cumulative product of gamma random variables whose prior expectation $E(\tau_s)$ increases with s when $a_2 > 1$. Guidelines on the choice of hyperparameter a_1 and a_2 can be found in Durante (2017) who presents a numerical method for checking that the global variances $\theta_s = 1/\tau_s$ are stochastically decreasing in s near zero, that is, $\Pr\{\theta_s \in (0, \theta]\}$ is non-decreasing in s for any θ in a small neighbourhood of zero.

The multiplicative gamma process prior does not place any mass at zero and so none of the A_s , and hence P_s , matrices are shrunk exactly to zero. We define the *effective order* p^* of the model as the value of $s \leq p_{\max}$ such that P_s fails a criterion for truncation to zero when $s = p^*$ but passes for $s = p^* + 1, \dots, p_{\max}$. Applying the truncation criterion to the standardised P_s matrices, rather than the unconstrained A_s matrices, allows classical theory from univariate time-series analysis to inform our judgement in a manner which is robust with respect to the scale of the data as well as its length and dimension m . Further details on the truncation criterion are provided in Section 4.2.

An alternative increasing shrinkage prior is the cumulative shrinkage process (CUSP) (Legramanti et al., 2020). However, our experience working with this prior suggests that, though sensible posterior inferences can be obtained in the analysis of simulated data, inference on the model order is very sensitive to the choice of prior hyperparameters in analyses involving real data. This suggests a lack of robustness to the kind of model misspecification that is inevitable in analyses of real time-series.

3.2 Joint prior

Denoting the collection of unknown hyperparameters in the multiplicative gamma process prior by $\boldsymbol{\vartheta}$, we adopt an overall prior specification of the form

$$\pi(\Sigma, A_1, \dots, A_{p_{\max}}, \boldsymbol{\vartheta}) = \pi(\Sigma)\pi(\boldsymbol{\vartheta}) \prod_{s=1}^{p_{\max}} \pi(A_s | \boldsymbol{\vartheta}). \quad (2)$$

Various options are available for the error variance matrix Σ and distributions which offer the property of invariance with respect to the order of the variables in the observation vector are discussed in Heaps (2023). In the applications in this paper, we use one such distribution, taking Σ to be inverse Wishart, with a scale matrix that has a common element on the diagonal and a common element off the diagonal.

4 Posterior inference

4.1 Posterior distribution

For $i \leq j$, denote by $\mathbf{y}_{i:j}$ the time-series $\mathbf{y}_i, \dots, \mathbf{y}_j$. The likelihood for a series of n observations, $\mathbf{y}_{1:n}$, from a zero-mean $\text{VAR}_m(p_{\max})$ process can be expressed as

$$p(\mathbf{y}_{1:n} | \Sigma, \Phi) = p(\mathbf{y}_{1:p_{\max}} | \Sigma, \Phi) \prod_{t=p_{\max}+1}^n p(\mathbf{y}_t | \mathbf{y}_{(t-p_{\max}): (t-1)}, \Sigma, \Phi)$$

in which $\mathbf{Y}_t | \mathbf{y}_{(t-p_{\max}): (t-1)}, \Sigma, \Phi \sim N_m(\sum_{i=1}^{p_{\max}} \phi_i \mathbf{y}_{t-i}, \Sigma)$ and the initial distribution is $(\mathbf{Y}_1^T, \dots, \mathbf{Y}_{p_{\max}}^T)^T | \Sigma, \Phi \sim N_{mp_{\max}}(\mathbf{0}, G)$. Here G is given by

$$G = \begin{pmatrix} \Gamma_0 & \Gamma_1 & \cdots & \Gamma_{p_{\max}-1} \\ \Gamma_1^T & \Gamma_0 & \cdots & \Gamma_{p_{\max}-2} \\ \vdots & \vdots & \ddots & \vdots \\ \Gamma_{p_{\max}-1}^T & \Gamma_{p_{\max}-2}^T & \cdots & \Gamma_0 \end{pmatrix},$$

where the matrices $\Gamma_0, \dots, \Gamma_{p_{\max}-1}$ are available as by-products of the recursive mapping between the partial autocorrelation matrices and the original model parameters.

Regarding the likelihood as a function of the new parameters and combining it with the prior (2) via Bayes theorem yields the posterior distribution as

$$\pi(\Sigma, A_1, \dots, A_{p_{\max}}, \boldsymbol{\vartheta} \mid \mathbf{y}_{1:n}) \propto \pi(\Sigma)\pi(\boldsymbol{\vartheta}) \prod_{s=1}^{p_{\max}} \pi(A_s \mid \boldsymbol{\vartheta})p(\mathbf{y}_{1:n} \mid \Sigma, A_1, \dots, A_{p_{\max}}). \quad (3)$$

As explained in Heaps (2023), the posterior distribution is a complicated function of the A_s , making it ill-suited to computational inference based on Gibbs sampling. Rather than appealing to conditional independence structure in the posterior for one-at-a-time parameter updates, Hamiltonian Monte Carlo (HMC) (Neal, 2011) uses information on the slope of the logarithm of the posterior density to generate global proposals that update all parameters simultaneously. We have found it efficient in sampling from the posterior (3) and use `cmdstanr` (Gabry and Cesnovar, 2021), a lightweight R interface to the Stan software (Carpenter et al., 2017), to implement the HMC algorithm. Stan requires users to write a program in the probabilistic Stan modelling language, the role of which is to provide instructions for computing the logarithm of the kernel of the posterior density function. The Stan software then automatically sets up a Markov chain simulation to sample from the resulting posterior. This includes calculation of the gradient of the logarithm of the posterior density, random initialisation of the chains, and the tuning of the sampler.

4.2 Truncation criterion

Following Bhattacharya and Dunson (2011), we choose to truncate P_s to a zero matrix if the absolute value of all of its elements lie below some threshold, say ε . In classical time-series analysis, the partial autocorrelation plot, with its associated confidence intervals, plays an important role in the choice of order for a univariate autoregression. Under the hypothesis that the process is $\text{AR}(p)$, the estimators for the partial autocorrelations of order $p+1, p+2, \dots$ based on a sample of size n are approximately independent with mean equal to zero and variance equal to $1/n$. As a guide, we therefore approximate the posterior for the m^2 components $p_{s,ij}$ of P_s under this hypothesis as independent $N(0, 1/n)$ random variables and then compute the quantile $q_m(\beta)$ such that $\Pr\{\max_{i,j} |p_{s,ij}| < q_m(\beta)\} = \beta$ for some large value of β and set the threshold $\varepsilon = q_m(\beta) = \Phi^{-1}\{(\beta^{1/m^2} + 1)/2\}/\sqrt{n}$. For example, in the applications in Sections 5 and 6, we use $\beta = 0.99$. By choosing the threshold in this way, we account for both the length and dimension of the data, in addition to operating on a parameter which is unit-free.

For each draw from the posterior, we can apply this criterion to determine the effective order p^* of the process. This can be summarised to yield a numerical approximation of the posterior for p^* which provides a proxy for the posterior for p .

5 Simulation experiments

Consider the idealised setting in which we know that the data were generated from a stationary vector autoregression of known order, p . In order to explore the behaviour of the posterior distribution for p^* in this context, we carried out simulation experiments that considered data generated from processes whose orders took various values. Our choice of truncation criterion makes allowance for the dimension of the observation vector m and the length of the time-series n . We might therefore expect some degree of robustness in the more challenging inferential situations when n is small or, in particular, when m is

large. This was investigated by considering simulations under a variety of values of m and n .

For each $m \in \{1, 3, 5, 7\}$ and $p \in \{1, 2, 3, 4\}$ we simulated ten sets of $m \times m$ matrices A_1, \dots, A_p with elements sampled independently from a standard normal distribution. Taking the error variance matrix to be $\Sigma = I_m$, these were used to simulate ten $\text{VAR}_m(p)$ processes of length $n = 1000$. Conditional on each data set, we then generated samples from the posterior distribution using Stan, as described in Section 4, setting the maximum possible order as $p_{\max} = 8$. Values for the other hyperparameters in the prior are detailed in the Supplementary Materials. In all cases, we used four chains each with 1000 iterations of warm-up followed by 4000 sampling iterations. Using the truncation criteria with $\beta = 0.99$, we calculated the limits $q_m(\beta)$ as 0.081, 0.103, 0.112 and 0.117 for $m = 1, 3, 5,$ and 7 respectively, and obtained a posterior mass function for the effective order p^* of each process. The posterior mass functions are summarised in Figure 1 across all simulation experiments. For a given (m, p) , the posteriors for the ten data sets are presented as a collection of overlaid bar charts. In nearly all cases, the true order p of the process is the mode in the posterior for p^* , with considerable posterior support. The results are similar across different values of m and p , suggesting robustness to the dimension of the data through our choice of truncation criteria.

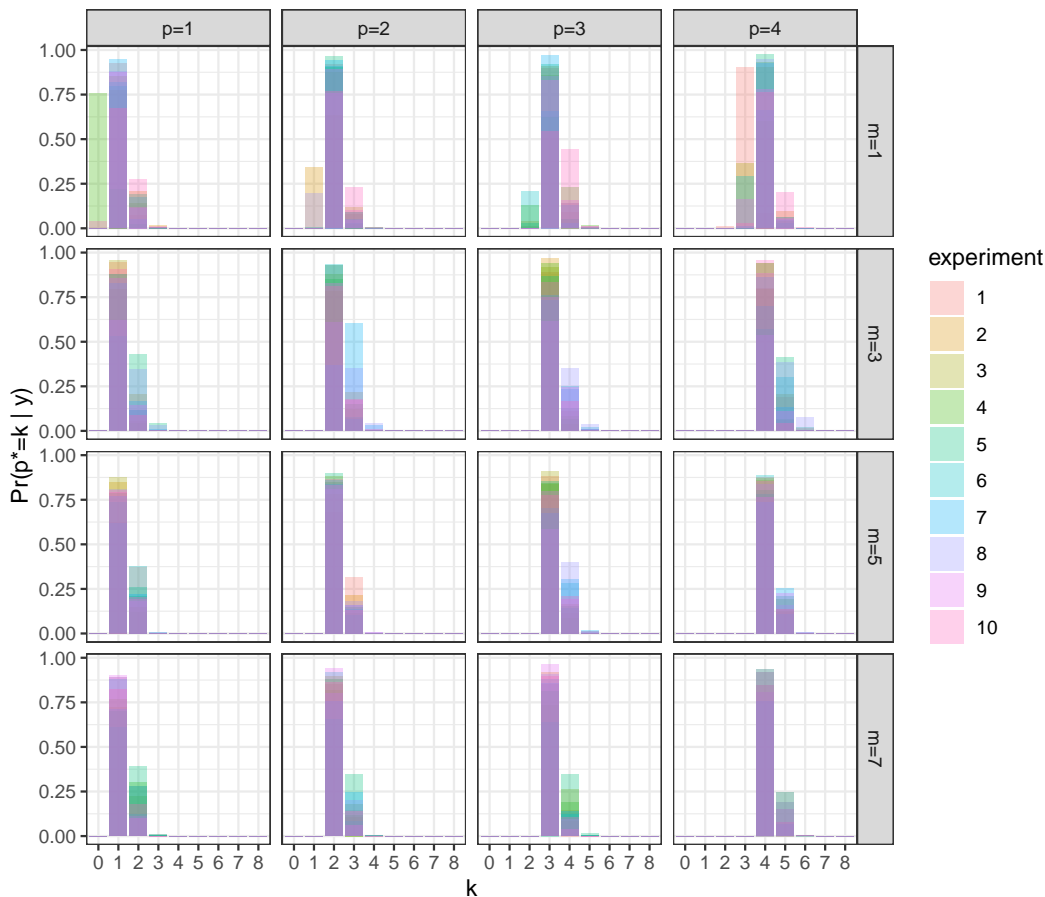


Figure 1: Overlaid posterior mass functions for the effective order p^* from 10 experiments for each combination of $m \in \{1, 3, 5, 7\}$ and $p \in \{1, 2, 3, 4\}$, with $n = 1000$.

Fixing $m = 3$, considering $p \in \{1, 2, 3, 4\}$ and using the same ten sets of matrices A_1, \dots, A_p as in the previous experiment, we then simulated ten $\text{VAR}_m(p)$ processes of length $n = 100$ and another ten of length $n = 500$, facilitating comparison across $n \in \{100, 500, 1000\}$. Retaining the same prior specification in the new experiments, we fit the model using HMC via Stan, as discussed above. Again, using the truncation criteria with $\beta = 0.99$ led to limits $q_m(\beta)$ equal to 0.326, 0.146 and 0.103 for $n = 100, 500$ and 1000, respectively. This yielded the posterior mass functions for p^* which are displayed in Figure 2. Across all experiments for the different values of n , the posterior mode for the effective order p^* recovers the true order p of the process, again, with considerable support. This holds for all values of n , suggesting robustness through the choice of truncation criteria, even for short time-series.

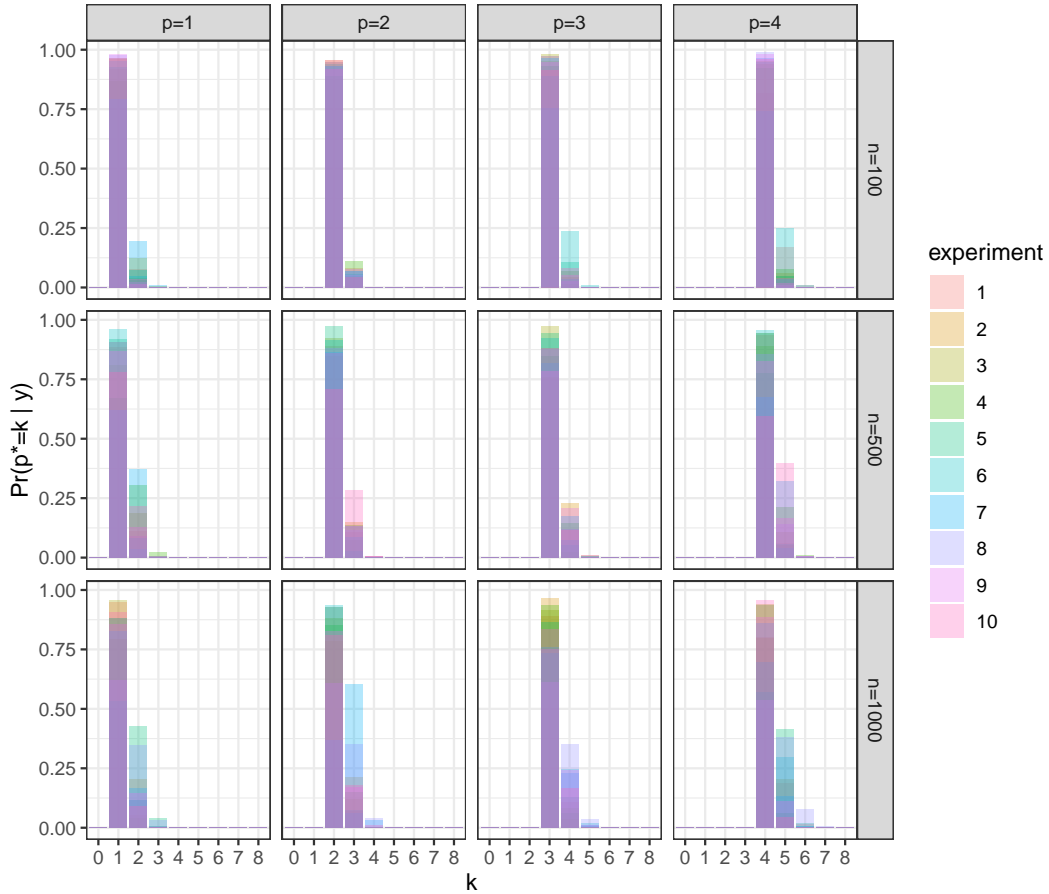


Figure 2: Overlaid posterior mass functions for the effective order p^* from 10 experiments for each combination of $n \in \{100, 500, 1000\}$ and $p \in \{1, 2, 3, 4\}$, with $m = 3$.

6 Application: understanding brain rhythms

6.1 Background

As an example application, we will apply our model and inferential procedures to a dataset of long-term intracranial EEG recordings to understand biological rhythms in the brain. Biological rhythms on ultradian, circadian, and longer timescales have been demonstrated in human physiology; but particularly the ultradian rhythms remain elusive in mechanism and function in the brain (Goh et al., 2019; Lloyd and Stupfel, 1991). Multiple lines of evidence suggest that some prominent ultradian rhythms exist in brain activity as measured by EEG (Hayashi et al., 1994; Panagiotopoulou et al., 2022), and may be related to rest-activity cycles, or even modulate disease symptoms.

In this exploratory application we investigate the properties that such ultradian biological rhythms may display in human brain activity. We use band power in two common frequency bands (delta and beta) as our features of interest.

6.2 Data preprocessing

Intracranial EEG recordings are considered from four subjects with refractory focal epilepsy from the University College London Hospital (UCLH). We give the individuals the anonymous identities of A, B, C and D. The nature of the recording was chosen for its high signal-to-noise ratio without the need for extensive artefact detection and removal.

Firstly, we divided each subject’s iEEG data into non-overlapping, consecutive segments of length 30 seconds. All channels within each segment were re-referenced to a common average reference. In the common average calculation, channels with extreme amplitude values were excluded. A notch filter was then applied at 50 Hz for each 30 second time window to remove line noise, after which the time windows were band-pass filtered from 0.5 – 80 Hz using a fourth order zero-phase Butterworth filter (second order forward and backward filter applied) and downsampled to 200 Hz.

Next, the iEEG data were decomposed into commonly studied frequency bands, including delta and beta (Taylor et al., 2022). We calculated the iEEG band power for each 30 second segment for all channels in two frequency bands (δ : 1 – 4 Hz, β : 13 – 30 Hz) using Welch’s method with three-second non-overlapping windows. After taking logarithms to base 10 of the band power recordings in each channel, the channels were averaged into the brain regions from which they were recorded based on the Desikan-Killiany atlas; see Wang et al. (2023) for further details. The number of brain regions varied between individuals, with $m = 9, 8, 8$ and 13 for individuals A, B, C and D respectively. Finally, the data were mean-centered prior to analysis.

For each individual we analysed the longest possible contiguous time period of their band power time-series for which graphical interrogation of the data suggested stationarity was a plausible assumption; therefore the length of the recording chosen for further analysis varied across subjects. The number of observations in the recordings used were $n = 651, 622, 685$ and 231 for individuals A, B, C and D respectively, equivalent to 5.417, 5.175, 5.7 and 1.917 hours. These recordings were obtained during day-time hours. We apply our model and inferential procedures to the time-series of both the beta and delta band power values for each individual, with a maximum order of $p_{\max} = 8$. The choices of hyperparameters in the prior are provided in the Supplementary Materials.

6.3 Order determination

For each of the individuals, the posterior distributions for p^* for both the beta and delta series were calculated using the truncation criteria described in Section 4.2 with $\beta = 0.99$. For example, in Figure 3, the posterior mass functions for the data pertaining to individual A are shown. For both the delta and beta series, the posterior mode is 2, with posterior support exceeding $2/3$. These results are quantitatively similar across all individuals, with corresponding figures displayed in the Supplementary Materials, possibly indicating similar generative processes for their ultradian rhythms.

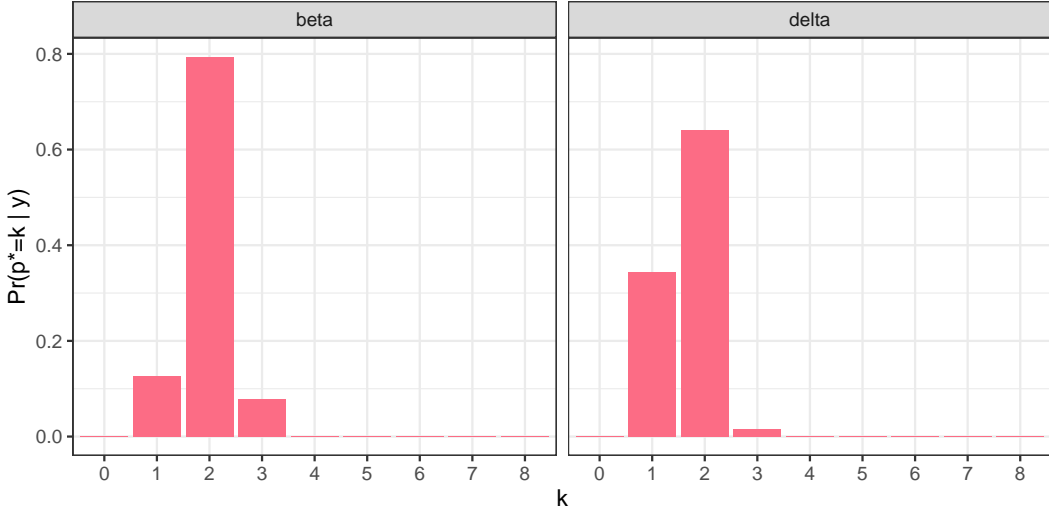


Figure 3: Posterior mass function for the order of process for the beta (left) and delta (right) series for individual A.

6.4 Granger causality

Conditioning on the modal order of the process for both series in each patient, we obtain samples from the posterior distributions of the autoregressive coefficient matrices. The (i, j) -th element in the autoregressive matrix at lag- s , $\phi_{s,ij}$, governs the effect of the j -th variable at time $t - s$ on the i -th variable at time t . If $\phi_{s,ij}$ is non-zero we say that variable j Granger-causes variable i at lag s ; this causal connection can be represented in a directed network, called a Granger causality plot, through an edge from vertex j to vertex i . Conditional on the posterior modal order, $p^* = 2$, Figures 4 and 5 show the Granger causality plots at lags 1 and 2 for individual A in the beta and delta bands, respectively. In these plots, an autoregressive coefficient is visualised as non-zero whenever zero lies outside the 50% equi-tailed Bayesian credible interval; the thickness of the edges representing non-zero coefficients are representations of the absolute value of the posterior mean. The coordinates of the vertices, representing the different brain regions, correspond to the x and y coordinates of the centre of the region using the Desikan-Killiany atlas. A noticeable feature of these Granger causality plots is the higher number of connections in the delta band compared to the beta band. This was common across all individuals (see Supplementary Materials), and may indicate more localised processes underpinning the delta rhythms that interact with each other, whereas the beta rhythms in each region may

be more driven by common processes. However future work has to confirm if this feature is a result of the epilepsy, or medication.

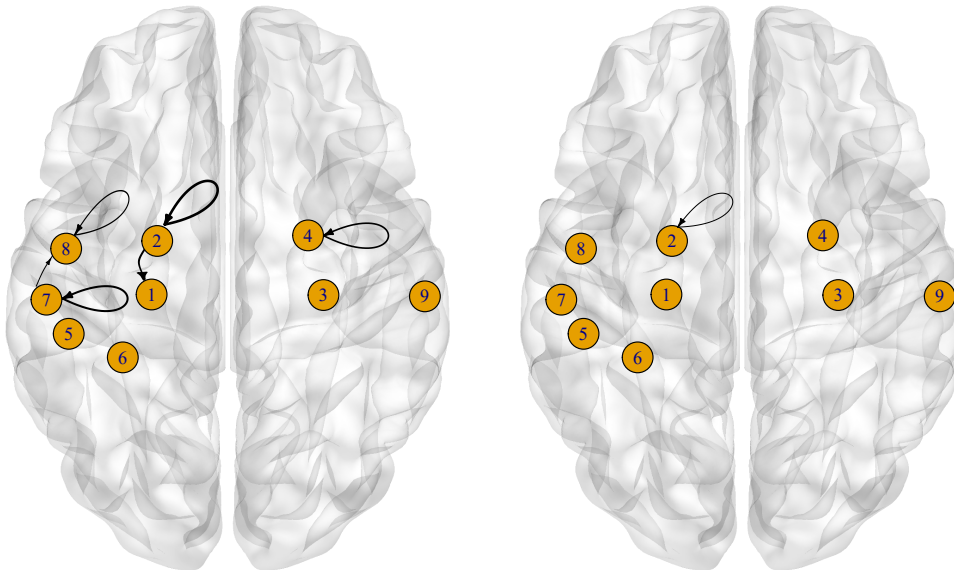


Figure 4: Granger causality plots of the posterior mean of the autoregressive coefficient matrices for the VAR process of individual A in the beta band at lag 1 (left) and lag 2 (right), overlaid on glass brains showing the locations of the regions. Region names: 1 - left-hippocampus, 2 - left-amygdala, 3 - right-hippocampus, 4 - right-amygdala, 5 - l.inferiortemporal, 6 - l.fusiform, 7 - l.middletemporal, 8 - l.superiortemporal, 9 - r.middletemporal.

6.5 Decomposition into latent series

Using classic theory of time-series decompositions (Prado, 1998), a $\text{VAR}_m(p)$ process can be decomposed into pm latent series. These series correspond to the pm distinct eigenvalues of the companion matrix which arises from the representation of the model as a $\text{VAR}_{mp}(1)$ process. Suppose there are c complex conjugate pairs of eigenvalues denoted $r_j e^{\pm i\omega_j}$, $j = 1, \dots, c$, and $pm - 2c$ real eigenvalues denoted r_j , $j = 2c + 1, \dots, pm$ where $r_j > 0$ and $\omega_j \in [0, \pi)$. The latent decomposition of $\mathbf{y}_t = (y_{t1}, \dots, y_{tm})^T$ then takes the form

$$y_{ti} = \sum_{j=1}^c z_{tij} + \sum_{j=2c+1}^{pm} x_{tij}$$

where z_{tij} and x_{tij} are real-valued processes corresponding to the j th pair of complex eigenvalues and the j th real eigenvalue, respectively. The process z_{tij} follows an ARMA(2,1) structure with AR coefficients $2r_j \cos \omega_j$ and $-r_j^2$ and is therefore quasi-periodic with characteristic frequency ω_j and modulus r_j . This holds for all dimensions $i = 1, \dots, m$, though the time-varying amplitude and phase are different for each i . Similarly, the process x_{tij} follows an AR(1) structure with coefficient r_j for all $i = 1, \dots, m$. Clearly the innovations that drive these latent ARMA(2,1) and AR(1) are correlated and arise from the error terms ϵ_t in the original model.

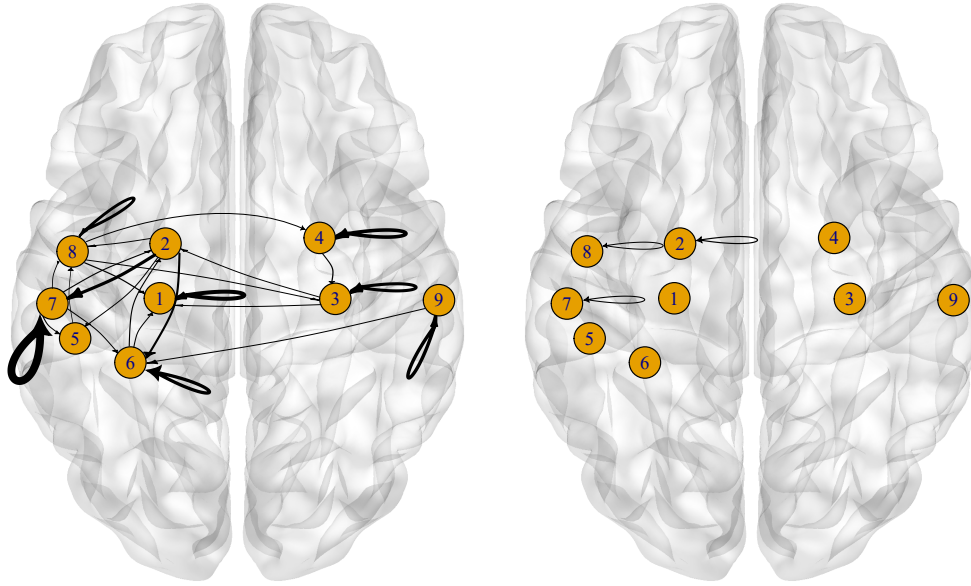


Figure 5: Granger causality plots of the posterior mean of the autoregressive coefficient matrices for the VAR process of individual A in the delta band at lag 1 (left) and lag 2 (right), overlaid on glass brains showing the locations of the regions. Region names: 1 - left-hippocampus, 2 - left-amygdala, 3 - right-hippocampus, 4 - right-amygdala, 5 - l.inferiortemporal, 6 - l.fusiform, 7 - l.middletemporal, 8 - l.superiortemporal, 9 - r.middletemporal.

The quasi-periodic series arising from the complex conjugate pairs of eigenvalues are of particular interest as they can capture the cyclical patterns that are key to understanding variation in brain activity. The pairs of complex eigenvalues, $r_j e^{\pm i\omega_j}$, $j = 1, \dots, c$, are not identifiable as the model remains unchanged under any permutation of their labelling. However, identification can be achieved by applying an ordering constraint, for example, based on the modulus or the argument. Imposing the constraint $\omega_1 < \omega_2 < \dots < \omega_c$, the quasi-periodic series z_{tij} are ordered by decreasing period $2\pi/\omega_j$.

For individual A the posteriors for the periods and moduli of the first four quasi-periodic series are presented in Figures 6 and 7. We note that the z_{tij} with highest period also have highest modulus and might therefore be regarded as the dominating latent series. Corresponding figures for the other individuals are provided in the Supplementary Materials. Across individuals, a common feature is that the posterior for the period of the dominating latent series in each band has its mean at around 20 minutes; for example, for individual A, the posterior means in the beta and delta bands are 19.61 and 26.92 minutes, with 95% equi-tailed Bayesian credible intervals of (3.86, 80.88) and (4.535, 111.871) minutes, respectively. It is also noticeable that though there are some differences between the moduli of the series in the delta band compared to the beta band, there is very little difference between the corresponding periods. Again, this feature is replicated across all individuals. We elaborate further on this observation in Section 7.

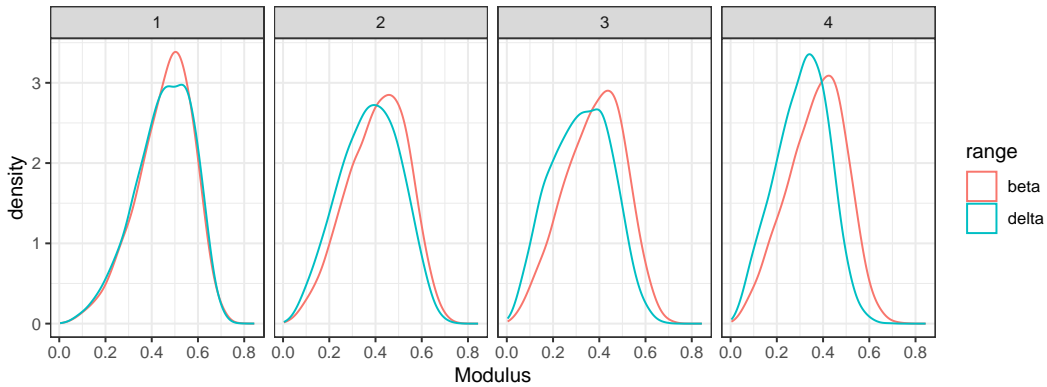


Figure 6: Posterior densities for the moduli of the first four quasi-periodic series for individual A.

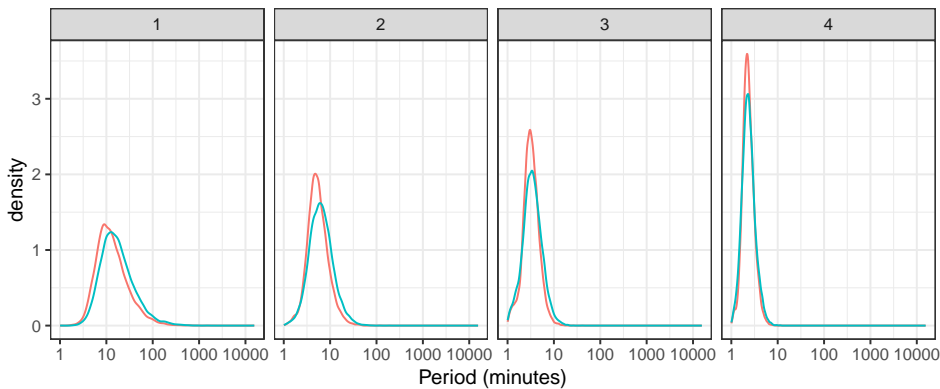


Figure 7: Posterior densities for the periods of the first four quasi-periodic series for individual A.

7 Discussion

We have proposed a hierarchical Bayesian model, with accompanying model-fitting methodology, which allows inference on the order of a stationary vector autoregression. This is based on an unconstrained reparameterisation of the stationary model in terms of a set of transformed partial autocorrelation matrices (Heaps, 2023) whose properties can be exploited in the design of the prior. In particular, we capitalise on the nested structure of the new parameterisation by constructing an overparameterised hierarchical model which shrinks unnecessary, high-order terms to zero; by identifying the lag beyond which the partial autocorrelation parameters become effectively equal to zero, we can then learn the order of the process. Further, using the relationship between the spectral norm of a partial autocorrelation matrix and its unconstrained counterpart, the prior is chosen to increasingly shrink the partial autocorrelation matrices at higher lags towards zero through a multiplicative gamma process for the unconstrained matrices.

An efficient Hamiltonian Monte Carlo sampler for computational inference was proposed and implemented through Stan, with accompanying code to allow easy dissemination

into other fields. The interpretability of the reparameterisation allowed use of classical theory on the distribution of the estimators of the partial autocorrelation function to make a judgement about which sampled partial autocorrelation matrices are approximately equal to zero. An associated truncation criteria determines the number of non-zero partial autocorrelation matrices, allowing posterior inference on the order of the process in a manner which accounts for the scale, dimension and length of the time-series.

We applied our methodology to a series of simulation experiments in which data sets of various lengths n were sampled from various stationary $\text{VAR}_m(p)$ models. For all values of m , p and n considered, the posterior for the effective order of the process was highly concentrated around the known model order. We then applied our methodology to iEEG data from recordings at various locations in the brain. Conditioning on the posterior modal order of these processes allowed physiological insight in a number of directions. By constructing Granger causality plots, we were able to highlight relationships between activity in different regions of the brain. Similarly, by constructing the latent decomposition of the series, we were able to identify underlying quasi-periodic structure. In particular, we found that the dominant latent component had a period that was around 20 minutes across all individuals in both the beta and the delta bands. This is consistent with ultradian rhythms of around 20 minutes which have previously been observed (Panagiotopoulou et al., 2022). The similarity in the periods across the beta and delta bands indicate that there is a global change in the band power pattern, rather than a local change within a specific band. The similarities between subjects are striking, particularly the period of 20 minutes, and warrants future investigations into the possible biological mechanisms and potentially endogenous drivers (Goh et al., 2019). However, as we only considered four subjects in this work, a larger study would be needed to confirm any biological interpretations, with a larger number of patients, longer recordings and accounting for the potential pathology present in these subjects.

An obvious limitation in the application to iEEG data was the necessity to pick out contiguous segments of data where stationarity was a plausible assumption. However, as remarked in Section 1, stationary autoregressions often serve as building blocks in the construction of more complex models. Motivated by applications involving iEEG data where subjects transition between states of wakefulness and sleep, or states of normal brain activity and seizure, we are currently exploring a hidden Markov model in which a (locally) stationary vector autoregression describes the within-state dynamics. Such a model would be ideally suited to a wide variety of time-series where there are occasional step-changes in a process which otherwise appears to be mean reverting.

Acknowledgements

This work was supported by the Engineering and Physical Sciences Research Council (EPSRC), Centre for Doctoral Training in Cloud Computing for Big Data (grant number EP/L015358/1). This work was also supported by the EPSRC (grant number EP/N510129/1) via the the Alan Turing Institute project “Streaming data modelling for real-time monitoring and forecasting”.

SUPPLEMENTARY MATERIAL

Supporting information: Further details on the prior specification for the simulated and EEG applications, as well as additional plots from the EEG application. (.pdf file)

Data, R code and Stan program: The simulated data from Section 5, R scripts for simulating data, running Stan and post-processing the Stan output, as well as the Stan program for fitting the model can be found at the GitHub repository <https://github.com/rachelbinks/Bayesian-VAR-order-determination>. (url)

References

- Barnett, G., R. Kohn, and S. Sheather (1996). Bayesian estimation of an autoregressive model using Markov chain Monte Carlo. *Journal of Econometrics* 74, 237–254.
- Bhattacharya, A. and D. B. Dunson (2011, June). Sparse Bayesian infinite factor models. *Biometrika* 98(2), 291–306.
- Carpenter, B., A. Gelman, M. Hoffman, D. Lee, B. Goodrich, M. Betancourt, M. Brubaker, J. Guo, P. Li, and A. Riddell (2017). Stan : A Probabilistic Programming Language. *Journal of Statistical Software* 76.
- Chiang, S., M. Guindani, H. J. Yeh, Z. Haneef, J. M. Stern, and M. Vannucci (2016). Bayesian vector autoregressive model for multi-subject effective connectivity inference using multi-modal neuroimaging data. *Human Brain Mapping* 38(3), 1311–1332.
- Durante, D. (2017). A note on the multiplicative gamma process. *Statistics & Probability Letters* 122, 198–204.
- Fan, J., K. Sitek, B. Chandrasekaran, and A. Sarkar (2022). Bayesian Tensor Factorized Vector Autoregressive Models for Inferring Granger Causality Patterns from High-Dimensional Multi-subject Panel Neuroimaging Data. *arXiv:2206.10757*.
- Gabry, J. and R. Cesnovar (2021). *cmdstanr: R Interface to ‘CmdStan’*. <https://mc-stan.org/cmdstanr>, <https://discourse.mc-stan.org>.
- Goh, G. H., S. K. Maloney, P. J. Mark, and D. Blache (2019). Episodic Ultradian Events—Ultradian Rhythms. *Biology* 8(1), 15.
- Hannaford, N. E., S. E. Heaps, T. M. Nye, T. P. Curtis, B. Allen, A. Golightly, and D. J. Wilkinson (2023). A sparse Bayesian hierarchical vector autoregressive model for microbial dynamics in a wastewater treatment plant. *Computational Statistics & Data Analysis* 179, 107659.
- Hayashi, M., K. Sato, and T. Hori (1994, October). Ultradian rhythms in task performance, self-evaluation, and EEG activity. *Perceptual and Motor Skills* 79(2), 791–800.
- Heaps, S. E. (2023). Enforcing stationarity through the prior in vector autoregressions. *Journal of Computational and Graphical Statistics* 32(1), 74–83.
- Heaps, S. E., M. Farrow, and K. J. Wilson (2020). Identifying the effect of public holidays on daily demand for gas. *Journal of the Royal Statistical Society: Series A (Statistics in Society)* 183(2), 471–492.
- Huerta, G. and R. Prado (2006). Structured priors for multivariate time series. *Journal of Statistical Planning and Inference* 136(11), 3802–3821.
- Huerta, G. and M. West (1999). Priors and Component Structures in Autoregressive Time Series Models. *Journal of the Royal Statistical Society. Series B (Statistical Methodology)* 61(4), 881–899.

- Jiang, X., X. Hu, W. Xu, G. Li, and Y. Wang (2013). Inference of microbial interactions from time series data using vector autoregression model. In *2013 IEEE International Conference on Bioinformatics and Biomedicine*, pp. 82–85.
- Koop, G. and D. Korobilis (2010). Bayesian multivariate time series methods for empirical macroeconomics. *Foundations and Trends in Econometrics* 3(4), 267–358.
- Legramanti, S., D. Durante, and D. B. Dunson (2020). Bayesian cumulative shrinkage for infinite factorizations. *Biometrika* 107(3), 745–752.
- Lloyd, D. and M. Stupfel (1991, August). The occurrence and functions of ultradian rhythms. *Biological Reviews of the Cambridge Philosophical Society* 66(3), 275–299.
- Neal, R. M. (2011). MCMC using Hamiltonian dynamics. In S. Brooks, A. Gelman, G. Jones, and X.-L. Meng (Eds.), *Handbook of Markov Chain Monte Carlo*, Handbooks of modern statistical methods, pp. 113–162. Chapman & Hall/CRC.
- Panagiotopoulou, M., C. A. Papasavvas, G. M. Schroeder, R. H. Thomas, P. N. Taylor, and Y. Wang (2022). Fluctuations in EEG band power at subject-specific timescales over minutes to days explain changes in seizure evolutions. *Human Brain Mapping* 43(8), 2460–2477.
- Prado, R. (1998). *Latent structure in non-stationary time series*. Ph. D. thesis, Duke University.
- Rousseau, J. and K. Mengersen (2011). Asymptotic behaviour of the posterior distribution in overfitted mixture models. *Journal of the Royal Statistical Society: Series B (Statistical Methodology)* 73(5), 689–710.
- Roy, A., T. McElroy, and P. Linton (2019). Constrained Estimation of Causal Invertible VARMA. *Statistica Sinica*.
- Taylor, P. N., C. A. Papasavvas, T. W. Owen, G. M. Schroeder, F. E. Hutchings, F. A. Chowdhury, B. Diehl, J. S. Duncan, A. W. McEvoy, A. Miserocchi, J. de Tisi, S. B. Vos, M. C. Walker, and Y. Wang (2022). Normative brain mapping of interictal intracranial EEG to localize epileptogenic tissue. *Brain* 145(3), 939–949.
- Vermaak, J., C. Andrieu, A. Doucet, and S. J. Godsill (2004). Reversible Jump Markov Chain Monte Carlo Strategies for Bayesian Model Selection in Autoregressive Processes. *Journal of Time Series Analysis* 25(6), 785–809.
- Wang, Y., G. M. Schroeder, J. J. Horsley, M. Panagiotopoulou, F. A. Chowdhury, B. Diehl, J. S. Duncan, A. W. McEvoy, A. Miserocchi, J. de Tisi, and P. N. Taylor (2023). Temporal stability of intracranial electroencephalographic abnormality maps for localizing epileptogenic tissue. *Epilepsia* 00, 1–11.
- Zhang, W., I. Cribben, S. Petrone, and M. Guindani (2021). Bayesian Time-Varying Tensor Vector Autoregressive Models for Dynamic Effective Connectivity. *arXiv:2106.14083*.

Supplementary information for “Bayesian inference on the order of stationary vector autoregressions”

Rachel L. Binks¹, Sarah E. Heaps^{*2}, Mariella Panagiotopoulou³, Yujiang Wang³,
and Darren J. Wilkinson²

¹School of Mathematics, Statistics and Physics, Newcastle University

²Department of Mathematical Sciences, Durham University

³School of Computing, Newcastle University

Abstract

Supplementary material contained in this note includes further details on the prior specification for the simulated and EEG applications, as well as additional plots from the EEG application.

S1 Simulation experiments

S1.1 Choice of hyperparameters in the prior

In the simulation experiments, we followed guidelines provided in Durante (2017) to choose the hyperparameters of the multiplicative gamma process prior, taking $a_1 = 2.5$ and $a_2 = 3$. Additionally, we set $a = 6$. These hyperparameter choices result in a marginal prior for the elements of the unconstrained A_s matrices which have variance of less than one. As discussed in the Supplementary Materials of Heaps (2023), this is necessary to avoid multimodality in the prior induced for the partial autocorrelation matrices. In the inverse Wishart distribution used as a prior for Σ , the scale matrix is taken as I_m and the degrees of freedom as $m + 4$, which ensures the variance is finite.

S2 Application: understanding brain rhythms

S2.1 Choice of hyperparameters in the prior

We used the same choice of hyperparameters for our prior during the application to neural activity data as during the simulation experiments; see Section S1.

S2.2 Order determination

Figure 3 in the main manuscript presented the posterior mass function for the effective order p^* of the both the delta and beta series for individual A. The corresponding plots for the other three individuals are presented in Figures S1–S3.

*Corresponding author: sarah.e.heaps@durham.ac.uk

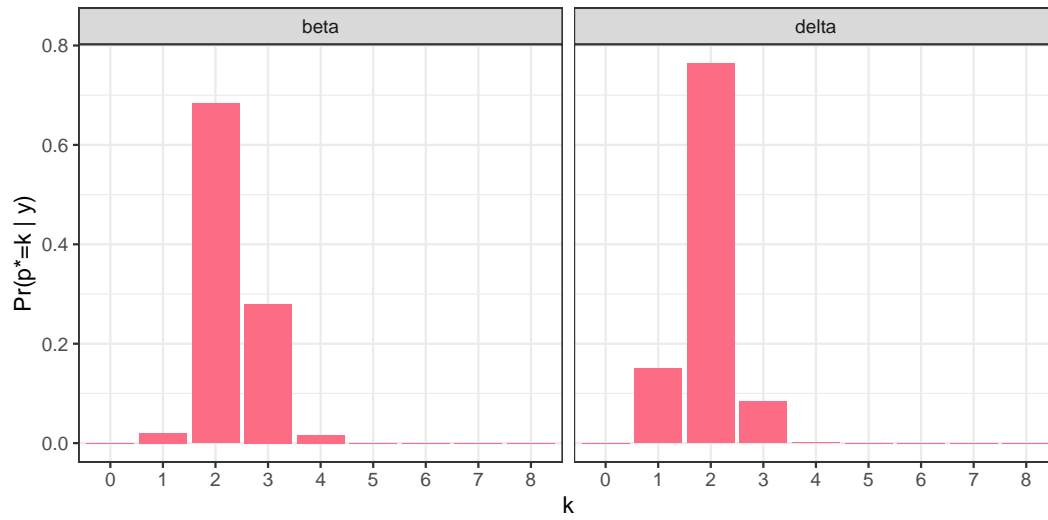


Figure S1: Posterior mass function for the order of the process for the beta (left) and delta (right) series for individual B.

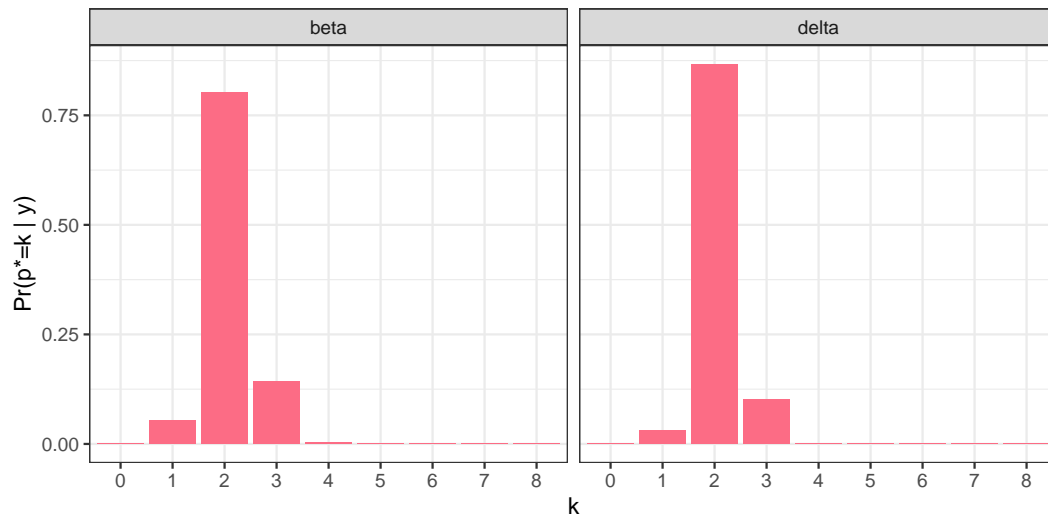


Figure S2: Posterior mass function for the order of the process for the beta (left) and delta (right) series for individual C.

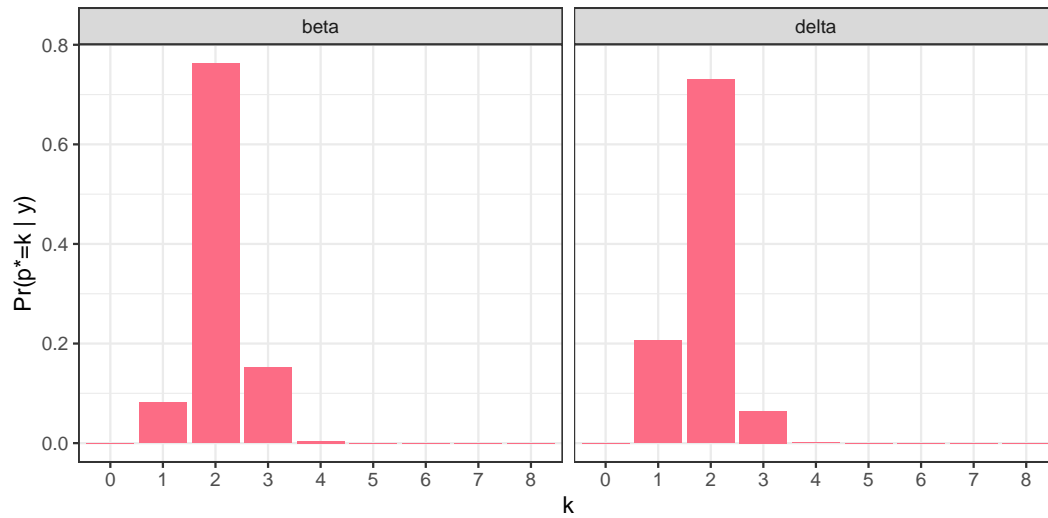


Figure S3: Posterior mass function for the order of the process for the beta (left) and delta (right) series for individual D.

S2.3 Granger causality

Figures 4 and 5 in the main manuscript display the Granger causality plots for individual A in the beta and delta bands. The corresponding plots for individuals B, C and D are presented in Figures S4–S5, S6–S7 and S8–S9, respectively. In all cases the mode of the posterior for p^* was equal to two and so we display graphs for lags 1 and 2 in each case.

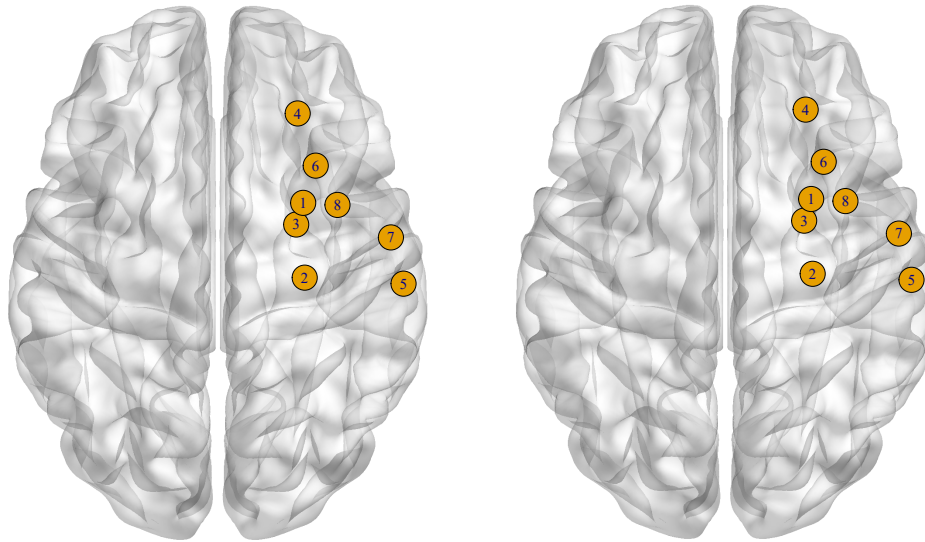


Figure S4: Granger causality plots of the posterior mean of the autoregressive coefficient matrices for the VAR process of individual B in the beta band at lag 1 (left) and lag 2 (right), overlaid on glass brains showing the locations of the regions. For this process, there are no elements of the autoregressive coefficient matrices for which zero lies outside of the relevant 50% equi-tailed Bayesian credible interval. Region names: 1 - right-putamen, 2 - right-hippocampus, 3 - right-amygdala, 4 - r.lateralorbitofrontal, 5 - r.middletemporal, 6 - r.temporalpole, 7 - r.superiortemporal, 8 - r.insula.

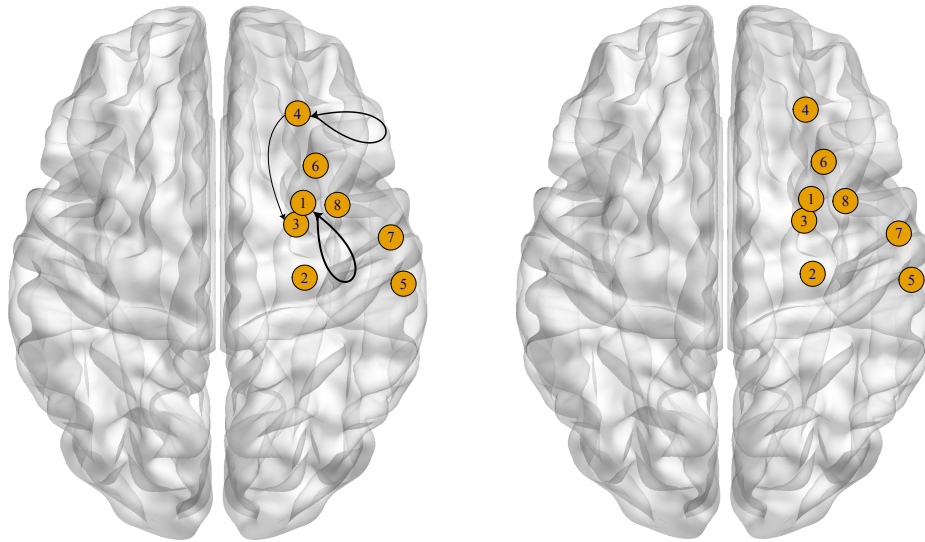


Figure S5: Granger causality plots of the posterior mean of the autoregressive coefficient matrices for the VAR process of individual B in the delta band at lag 1 (left) and lag 2 (right), overlaid on glass brains showing the locations of the regions. Region names: 1 - right-putamen, 2 - right-hippocampus, 3 - right-amygdala, 4 - r.lateralorbitofrontal, 5 - r.middletemporal, 6 - r.temporalpole, 7 - r.superiortemporal, 8 - r.insula.

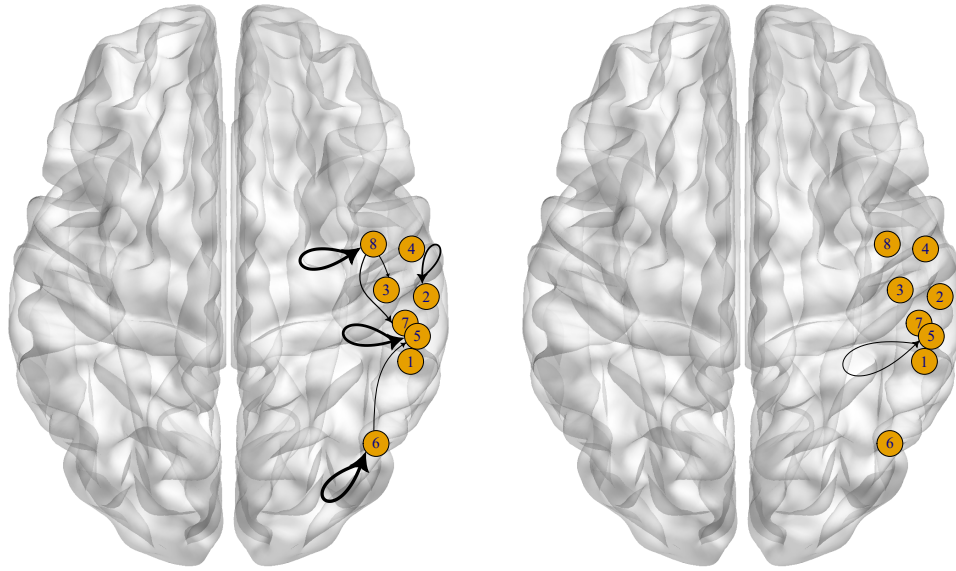


Figure S6: Granger causality plots of the posterior mean of the autoregressive coefficient matrices for the VAR process of individual C in the beta band at lag 1 (left) and lag 2 (right), overlaid on glass brains showing the locations of the regions. Region names: 1 - r.bankssts, 2 - r.middletemporal, 3 - r.postcentral, 4 - r.superiortemporal, 5 - r.supramarginal, 6 - r.inferiorparietal, 7 - r.inferiortemporal, 8 - r.precentral.

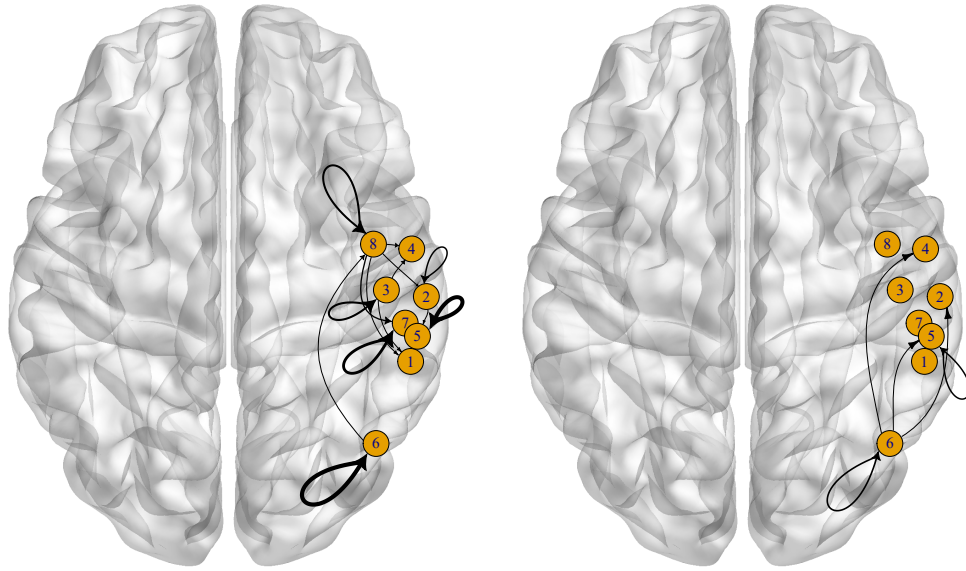


Figure S7: Granger causality plots of the posterior mean of the autoregressive coefficient matrices for the VAR process of individual C in the delta band at lag 1 (left) and lag 2 (right), overlaid on glass brains showing the locations of the regions. Region names: 1 - r.bankssts, 2 - r.middletemporal, 3 - r.postcentral, 4 - r.superiortemporal, 5 - r.supramarginal, 6 - r.inferiorparietal, 7 - r.inferiortemporal, 8 - r.precentral.

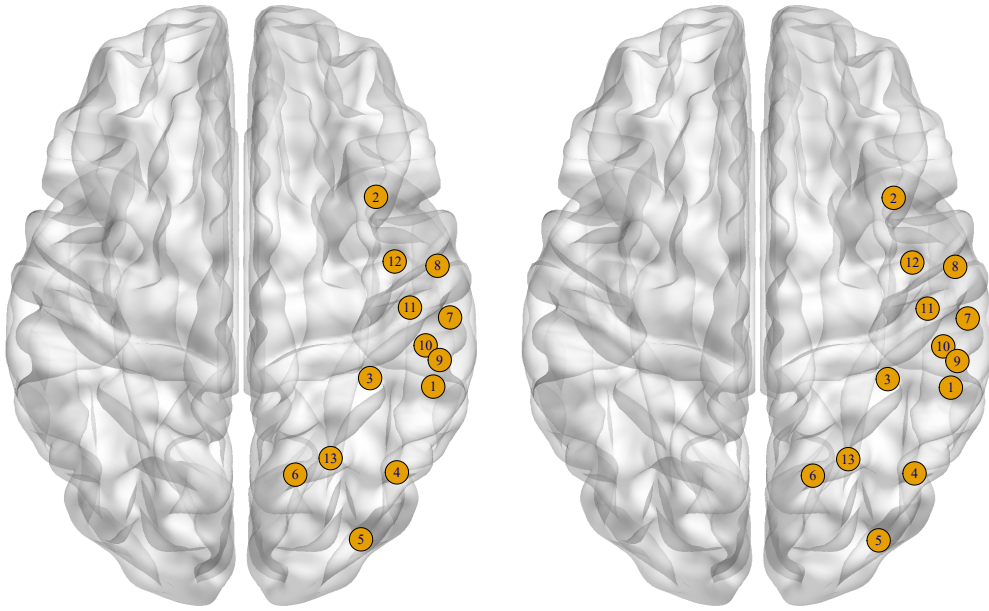


Figure S8: Granger causality plots of the posterior mean of the autoregressive coefficient matrices for the VAR process of individual D in the beta band at lag 1 (left) and lag 2 (right). For this process, there are no elements of the autoregressive coefficient matrices for which zero lies outside of the relevant 50% equi-tailed Bayesian credible interval. Region names: 1 - r.bankssts, 2 - r.caudalmiddlefrontal, 3 - r.fusiform, 4 - r.inferiorparietal, 5 - r.lateraloccipital, 6 - r.lingual, 7 - r.middletemporal, 8 - r.superiortemporal, 9 - r.supramarginal, 10 - r.inferiortemporal, 11 - r.postcentral, 12 - r.precentral, 13 - r.superiorparietal.

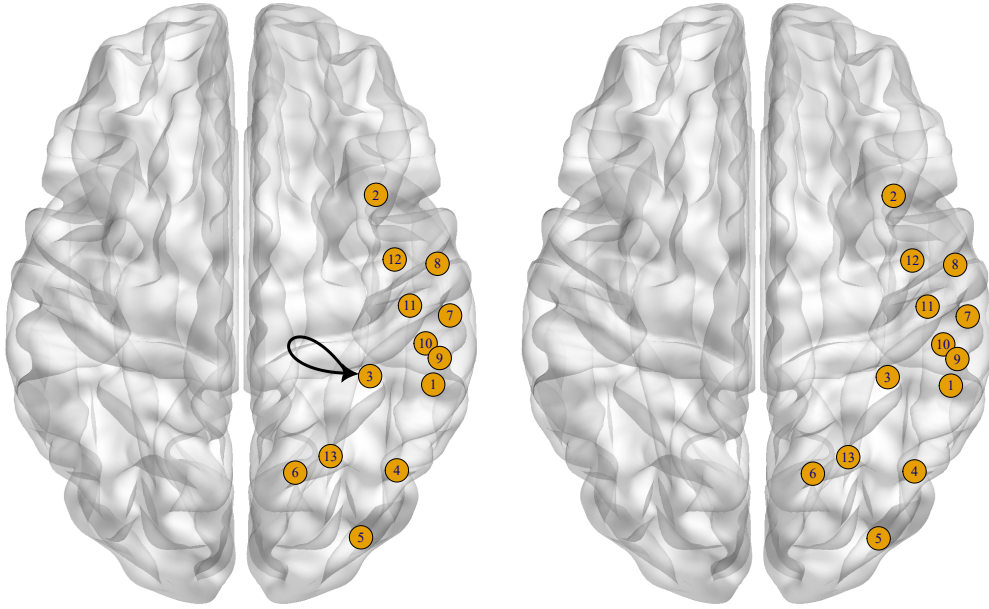


Figure S9: Granger causality plots of the posterior mean of the autoregressive coefficient matrices for the VAR process of individual D in the delta band at lag 1 (left) and lag 2 (right). Region names: 1 - r.bankssts, 2 - r.caudalmiddlefrontal, 3 - r.fusiform, 4 - r.inferiorparietal, 5 - r.lateraloccipital, 6 - r.lingual, 7 - r.middletemporal, 8 - r.superiortemporal, 9 - r.supramarginal, 10 - r.inferiortemporal, 11 - r.postcentral, 12 - r.precentral, 13 - r.superiorparietal.

S2.4 Latent moduli and periods

In the main manuscript, Figures 6 and 7 display the posterior densities for the moduli and periods of the first four quasi-periodic latent series for individual A. Corresponding plots for individuals B, C and D are presented in Figures S10–S11, S12–S13 and S14–S15, respectively.

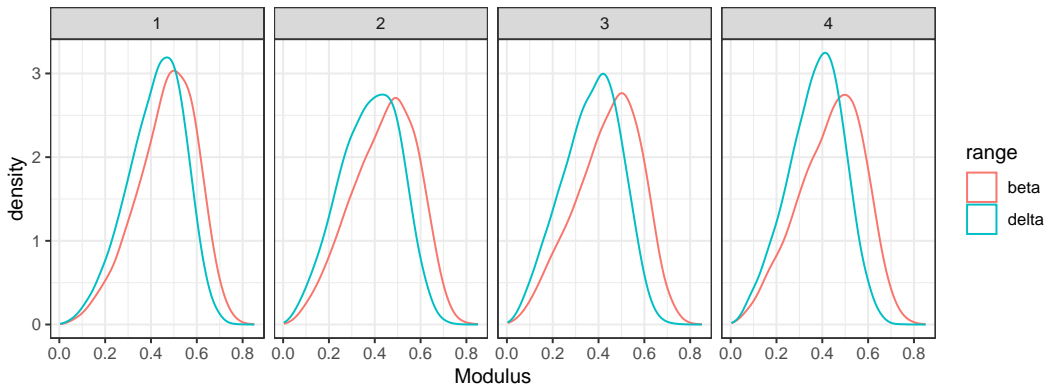


Figure S10: Posterior densities for the moduli of the first four quasi-periodic series for individual B.

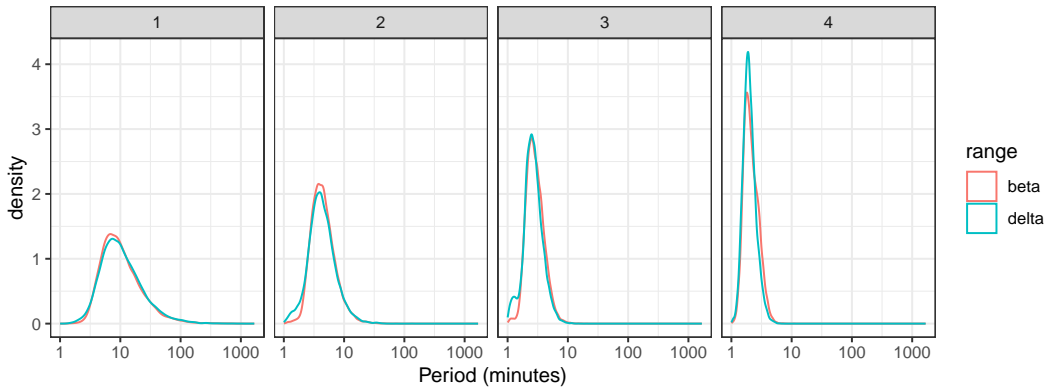


Figure S11: Posterior densities for the periods of the first four quasi-periodic series for individual B.

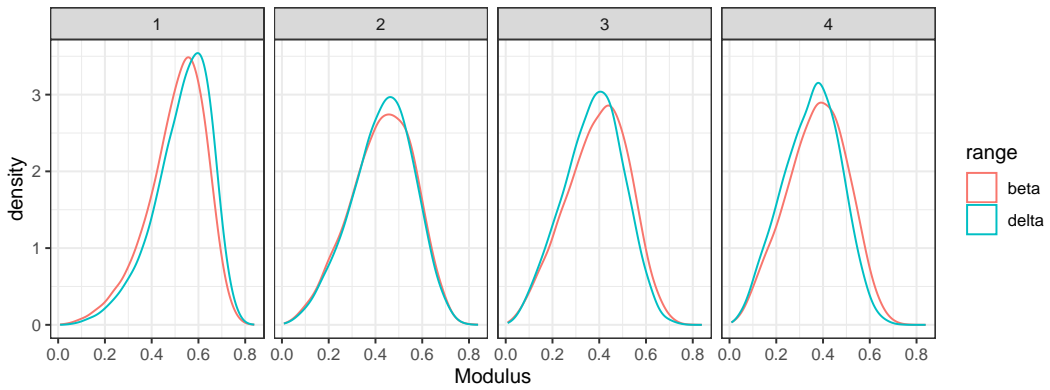


Figure S12: Posterior densities for the moduli of the first four quasi-periodic series for individual C.

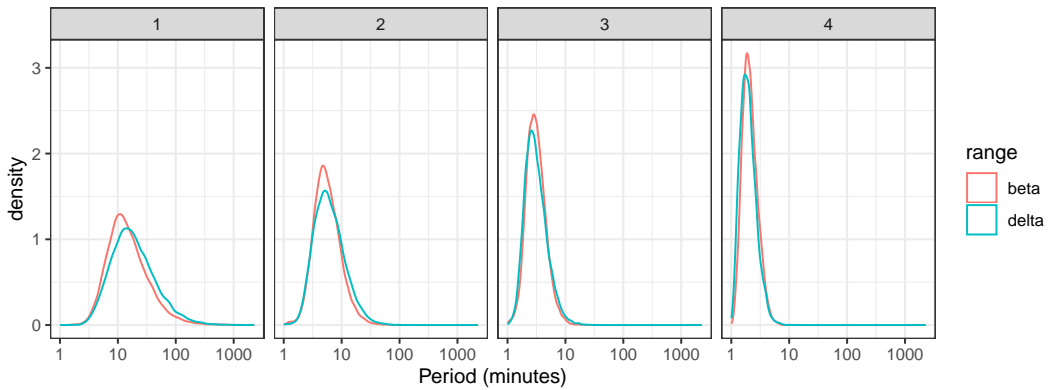


Figure S13: Posterior densities for the periods of the first four quasi-periodic series for individual C.

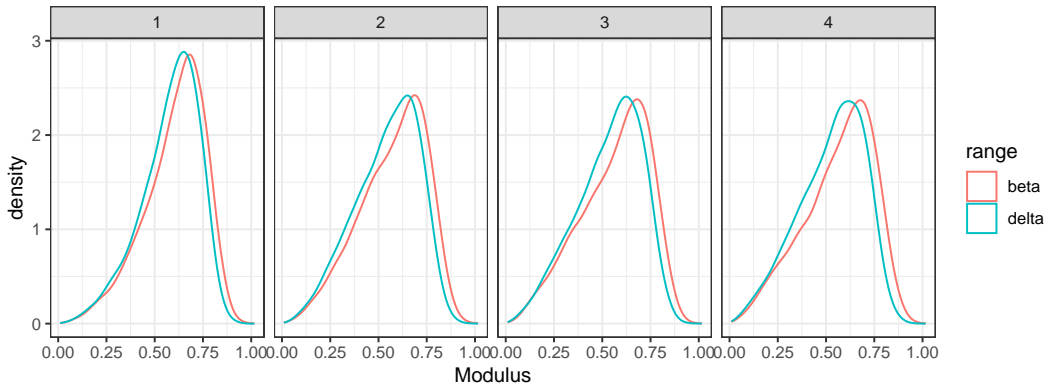


Figure S14: Posterior densities for the moduli of the first four quasi-periodic series for individual D.

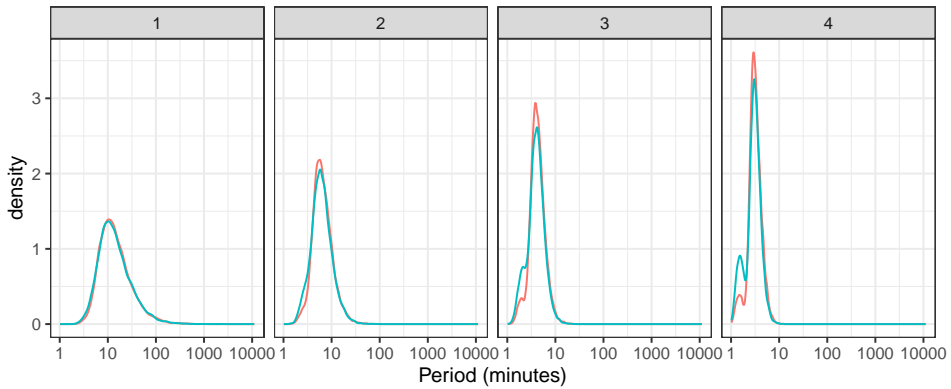


Figure S15: Posterior densities for the periods of the first four quasi-periodic series for individual D.

References

- Durante, D. (2017). A note on the multiplicative gamma process. *Statistics & Probability Letters* 122, 198–204.
- Heaps, S. E. (2023). Enforcing stationarity through the prior in vector autoregressions. *Journal of Computational and Graphical Statistics* 32(1), 74–83.